Computational and Structural Biotechnology Journal 21 (2023) 2688–2695

Contents lists available at ScienceDirect

Computational and Structural Biotechnology Journal

journal homepage: www.elsevier.com/locate/csbj

Research article

# A coarse-grained molecular dynamics investigation on spontaneous binding of $A\beta_{1-40}$ fibrils with cholesterol-mixed DPPC bilayers

Nikhil Agrawal [a,b,*], Adam A. Skelton [b], Emilio Parisini [a,c,*]

[a] Latvian Institute of Organic Synthesis, Aizkraukles 21, LV, Riga 1006, Latvia
[b] College of Health Sciences, University of KwaZulu-Natal, Durban, South Africa
[c] Department of Chemistry "G. Ciamician", University of Bologna, Via Selmi 2, 40126 Bologna, Italy

ARTICLE INFO

*Article history:*
Received 24 November 2022
Received in revised form 14 April 2023
Accepted 14 April 2023
Available online 15 April 2023

*Keywords:*
Alzheimer's disease
Amyloid
Cholesterol
DPPC
Lipid membrane
MD simulations

ABSTRACT

Alzheimer's disease is the most common form of dementia. Its aetiology is characterized by the misfolding and aggregation of amyloid-β (Aβ) peptides into β-sheet-rich Aβ oligomers/fibrils. Although multiple experimental studies have suggested that Aβ oligomers/fibrils interact with the cell membranes and perturb their structures and dynamics, the molecular mechanism of this interaction is still not fully understood. In the present work, we have performed a total of 120 μs-long simulations to investigate the interaction between trimeric or hexameric $A\beta_{1-40}$ fibrils with either a 100% DPPC bilayer, a 70% DPPC-30% cholesterol bilayer or a 50% DPPC-50% cholesterol bilayer. Our simulation data capture the spontaneous binding of the aqueous $A\beta_{1-40}$ fibrils with the membranes and show that the central hydrophobic amino acid cluster, the lysine residue adjacent to it and the C-terminal hydrophobic residues are all involved in the process. Moreover, our data show that while the $A\beta_{1-40}$ fibril does not bind to the 100% DPPC bilayer, its binding affinity for the membrane increases with the amount of cholesterol. Overall, our data suggest that two clusters of hydrophobic residues and one lysine help $A\beta_{1-40}$ fibrils establish stable interactions with a cholesterol-rich DPPC bilayer. These residues are likely to represent potential target regions for the design of inhibitors, thus opening new avenues in structure-based drug design against Aβ oligomer/fibril-membrane interaction.



## 1. Introduction

Amyloid fibrils are misfolded, β-sheet-rich, aggregated proteins that play a key role in more than 20 diseases, including Alzheimer's disease (AD), Parkinson's disease (PD), type 2 diabetes, HIV, and different forms of systemic amyloidosis [1–7]. Conditions involving amyloid fibrils formation, which are commonly known as protein misfolding diseases, affect millions of people around the world [8,9]. According to the amyloid cascade hypothesis, in the brain of AD patients the amyloid β peptide (Aβ) undergoes conformational changes to form water-insoluble Aβ fibrils [10,11]. These Aβ fibrils then form extracellular neuronal plaques, which represent the major pathological hallmark of AD [12,13].

Several experimental studies have been performed to reveal the effect of the interaction between Aβ fibrils and lipids/membranes. Han et al. used electron tomography to visualize the interaction of Aβ fibrils with lipids of different sizes, also reporting that intracellular fibrils deform the structure of intracellular lipid vesicles and puncture through the vesicular membrane into the cytoplasm [14]. Using simultaneous coherent anti-Stokes Raman scattering (CARS) and 2-photon fluorescence microscopy, Kiskis et al. showed that lipids co-localize with fibrillar β-amyloid (Aβ) plaques [15]. In another experimental study, Burns et al. revealed the co-localization of cholesterol in Aβ plaques [16]. Previously, several MD simulation studies were also done to investigate the interaction between membranes and Aβ oligomers/fibrils. For instance, Yu et al. performed MD simulations of the interaction between $A\beta_{17-42}$ fibrils and a mixed anionic POPC–POPG bilayer [17]. Their study showed that anionic lipids play an important role in the absorption of the $A\beta_{17-42}$ pentamer in the membrane. Tofoleanu et al. conducted MD simulations of the interaction between Aβ fibrils and a POPE lipid bilayer, and their data revealed that the charged residues Glu22, Asp23 and

* Corresponding authors at: Latvian Institute of Organic Synthesis, Aizkraukles 21, LV, Riga 1006, Latvia.
*E-mail addresses:* nikhil.08oct@gmail.com (N. Agrawal), emilio.parisini@osi.lv (E. Parisini).

https://doi.org/10.1016/j.csbj.2023.04.013

Lys28 form electrostatic interactions with head group atoms of the lipid [18]. In another study, Tofoleanu et al. used MD simulations to investigate the behaviour of Aβ fibrils with POPC and POPE bilayers [19]. This study revealed that Aβ fibrils form short-lived contacts with POPC head groups and strong contacts with POPE head groups. Dong et al. performed MD simulations of $A\beta_{40}$ fibril trimers with a POPG bilayer, revealing that their interaction is mediated by the N-terminal β-sheet [20]. In a recent work, Dias et al. used coarse-grained (CG) simulations to investigate the binding of $A\beta_{1-42}$ fibrils with a cholesterol-rich phosphatidylcholine (PC) bilayer, showing that 30% cholesterol is optimal for $A\beta_{1-42}$ fibril interaction with the membrane and that increasing the cholesterol content in PC bilayer up to 50% does not increase the binding frequency of $A\beta_{1-42}$ fibrils with the membrane [21].

It is well established that Aβ fibrils are highly polymorphic in nature and that their two isoforms, $A\beta_{1-40}$ and $A\beta_{1-42}$, show different structural features at the molecular level [22]. Moreover, Aβ fibrils structures have been reported to feature some degree of polymorphism within the same isoform; indeed, Meinhardt et al. showed that $A\beta_{1-40}$ fibrils form different structures even within the same sample and under the same conditions [23]. Hence, this highlights the importance of investigating also the interaction of $A\beta_{1-40}$ fibrils with lipid membranes. In the present study, we aimed to capture the spontaneous binding of the $A\beta_{1-40}$ fibril hexamer and trimer with cholesterol-rich dipalmitoylphosphatidylcholine (DPPC) bilayer. To this end, we performed sixty independent coarse-grained MD simulations to investigate the interaction of either trimeric or hexameric $A\beta_{1-40}$ fibrils with lipid bilayers of different compositions (100% DPPC, 70% DPPC-30% cholesterol, and 50% DPPC-50% cholesterol). The total simulation time was 120 μs (2 μs per run). This allowed us to assess how different concentrations of cholesterol affect the spontaneous binding of trimeric and hexameric $A\beta_{1-40}$ fibrils to the membrane, to identify the nature of the amino acids that are involved in the binding and to determine how the binding process affects fibril solvation in the proximity of the bilayer.

## 2. Methods

### 2.1. Structures and force field of Aβ fibrils and DPPC-cholesterol membranes

To perform CG molecular dynamics simulations, we used the NMR structure of a hexameric $A\beta_{9-40}$ fibril (PDB id: 2LMN) [24] and the cryo-electron microscopy (cryo-EM) structure of a trimeric $A\beta_{10-40}$ fibril (PDB id: 6W0O) [25] obtained from the cortical tissue of an AD patient. The atomistic structures of both the hexamer and the trimer were converted into a CG model (Fig. 1) using the CHARMM-GUI Martini maker [26,27] and the N-terminal residues that were missing in both models were added using the CHARMM-GUI model missing residues option. Membrane bilayers of different compositions (100% DPPC, 70% DPPC-30% cholesterol and 50% DPPC-50% cholesterol) were prepared using the CHARMM-GUI membrane bilayer builder option. Table 1 shows the initial number of lipid molecules in each type of membrane. Prior to starting the simulations on the fibril-membrane complexes, membranes were equilibrated for 200 ns each and the average area per lipid was calculated for the last 50 ns for each simulation (Supplementary Table 1).

The Martini 2.2 protein force field [28] was used for the $A\beta_{1-40}$ fibrils, while the Martini 2.0 force field was used for the membrane, water and ions [29].

### 2.2. Simulation protocol

We studied a total of six $A\beta_{1-40}$ fibril-membrane systems. System one contained one $A\beta_{1-40}$ fibril hexamer, a 100% DPPC bilayer and 49905 water molecules. System two contained one $A\beta_{1-40}$ fibril hexamer, a 70% DPPC-30% cholesterol bilayer and 37445 water molecules. System three contained one $A\beta_{1-40}$ fibril hexamer, a 50% DPPC-50% cholesterol bilayer and 32478 water molecules. A total of 18 $NA^+$ ions were added in these three systems to neutralize the overall charge. System four contained one $A\beta_{1-40}$ fibril trimer, a 100% DPPC bilayer and 50081 water molecules. System five contained one $A\beta_{1-40}$ fibril trimer, a 70% DPPC-30% cholesterol bilayer and 37608 water molecules. System six contained one $A\beta_{1-40}$ fibril trimer, a 50% DPPC-50% cholesterol bilayer and 32699 water molecules. A total of 9 $NA^+$ were added to neutralize the overall charge of these three systems. Initially, all six systems were energy-minimized using the steepest descent algorithm [30]. All systems were equilibrated in five cycles, with decreasing restrains in each cycle from force constant 1000 kJ $mol^{-1}$ $nm^{-2}$ in the first cycle to 50 kJ $mol^{-1}$ $nm^{-2}$ in the last cycle on the $A\beta_{1-40}$ fibril and from 20 kJ $mol^{-1}$ $nm^{-2}$ in the first cycle to 10 kJ $mol^{-1}$ $nm^{-2}$ in the last cycle on the lipid head groups. Equilibration was performed for a total of 4750 ps. All production simulations were done without any restraints on the $A\beta_{1-40}$ fibrils and membranes. The Parrinello-Rahman algorithm [31] with semi-isotropic pressure coupling type was used for pressure coupling and the velocity-rescale algorithm [32] was used for temperature coupling. Pressure coupling and temperature bath times were set at 12.0 ps and 1.0 ps, respectively. All simulations were performed at the temperature of 310.15 K and at the pressure of 1 atm. A 30 fs time step was used for the integration of Newton's equations of motion. A cut-off of 1.1 nm was employed for Van der Waals (VdW) and electrostatic interactions, and electrostatic interactions were treated using the reaction field method. A total of 60 independent simulations were done using an initial random velocity generated by GROMACS 2021 [33]. Each simulation was performed for 2 μs using GROMACS 2021 simulation package [33].

### 2.3. Analysis details

The minimum distance of the $A\beta_{1-40}$ fibril residues from the membrane was calculated using the GROMACS minidist program. An interaction with an $A\beta_{1-40}$ fibril residue was taken into account when the minimum distance between membrane lipids (either DPPC or cholesterol) and the residue was ≤ 5 Å. The minimum distance between each residue and the membrane was calculated within the time range of 0–2 μs. The number of water and lipid molecules was calculated within 6 Å of the $A\beta_{1-40}$ fibril. Area per lipid was calculated using FATSLiM [34] and VdW and electrostatic interaction energies were calculated using GROMACS mdrun program.

## 3. Results

### 3.1. Binding of the $A_{1-40}$ fibrils with the membranes

Cytotoxicity of amyloid fibrils is generally reported to their binding with cell membranes [35,36]. To see the spontaneous binding of $A\beta_{1-40}$ fibrils (hexamer and trimer) with the membrane, we calculated the time evolution of the minimum distance between hexamer and trimer with all three bilayers (Fig. 2). We observed no spontaneous binding in any of the 20 independent trajectories (10 each for the $A\beta_{1-40}$ hexamer and trimer, Fig. 2A, D) with the 100% DPPC bilayer. Indeed, although at times fibrils came close to the DPPC bilayer to establish some transient interactions, the distance between the fibrils and the membrane remained ≥ 5 Å for most of the simulation time. Conversely, out of 20 independent trajectories of the $A\beta_{1-40}$ fibrils with the membrane containing 70% DPPC and 30% cholesterol (Fig. 2B, E), in two trajectories of the trimeric $A\beta_{1-40}$ fibrils (SIM3 and SIM10), we observed stable binding with the membrane. In particular, the $A\beta_{1-40}$ trimer was found within 5 Å from the membrane for around ~0.915 μs and ~0.575 μs in SIM3 and SIM10, respectively. In both of these

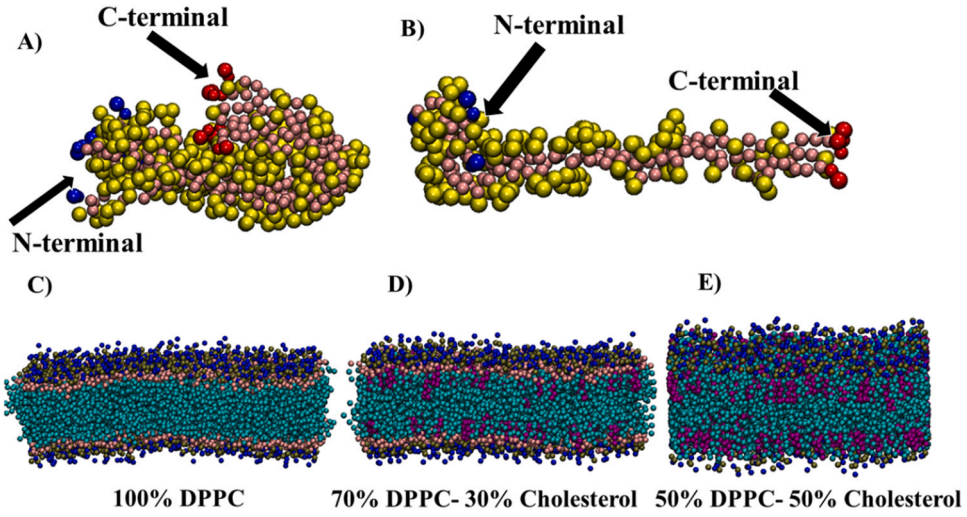


**Fig. 1.** A) CG model of the $A\beta_{1-40}$ fibril hexamer (PDB id: 2LMN). B) CG model of the $A\beta_{1-40}$ fibril trimer (PDB id: 6W0O). C) 100% DPPC membrane bilayer. D) 70% DPPC- 30% cholesterol membrane bilayer D) 50% DPPC- 50% cholesterol membrane bilayer. CG models of fibrils are shown using VdW representations, while backbone beads of fibrils are shown in pink colour, side chain beads are shown in yellow colour, N-terminal Asp1 residue is shown in blue colour and C-terminal Val40 is shown in red colour. The head group beads NC3 and PO4 of the DPPC molecules are illustrated in blue and tan, respectively, while the head group of cholesterol molecules is colored maroon. The tails of both lipid molecules are depicted in cyan.

simulations, the trimer remained bound to the membrane until the end of the simulation time. In all other trajectories, only transient interactions with the membrane were noted. When considering a 50% DPPC-50% cholesterol membrane (Fig. 2C, E), we observed stable binding in 6 out of 10 trajectories with the $A\beta_{1-40}$ hexamer (SIM1, SIM4, SIM7, SIM8, SIM9, and SIM10), while stable binding was observed in 5 out of 10 trajectories with the $A\beta_{1-40}$ trimer (SIM1, SIM4, SIM5, SIM6, SIM9). The longest binding time was detected in SIM1 and SIM4 for the hexamer simulations, and in SIM4 and SIM9 for the trimer simulations. In all these 4 simulations, $A\beta_{1-40}$ fibrils were found to bind with the membrane for more than 50% of the total simulation time.

To further evaluate the distribution of minimum distances in all the simulations, we constructed violin plots for both types of fibrils with all three different bilayers (Fig. 3). The violin plot of the hexameric $A\beta_{1-40}$ fibril shows a high density of values within 5 Å for the bilayer containing 50% cholesterol (Fig. 3A, red colour). In the case of the trimer (Fig. 3B), the highest density of less than 5 Å distances is also seen when considering the membrane containing 50% cholesterol (Fig. 3B, red colour), followed by the membrane containing 30% cholesterol (Fig. 3B, blue colour). Violin plots also reveal a decrease in minimum distance values in going from 0% cholesterol to 50% cholesterol in the membrane for both types of fibrils. Fig. 4 shows $A\beta_{1-40}$ fibrils (hexamer and trimer) with a membrane containing 50% DPPC and 50% cholesterol at four different time points in two representative trajectories.

Overall, these data suggest that, if we exclude some transient interactions, $A\beta_{1-40}$ fibrils (either hexamer or trimer) show little to no affinity for cholesterol-free membranes. However, when the cholesterol level increases to 50% both types of fibrils bind stably to the membrane. Moreover, $A\beta_{1-40}$ fibrils can also bind firmly with the membrane when 30% cholesterol is present, as seen in trimer simulations.

### 3.2. Identification of membrane binding residues

To identify which residues bind to the membrane, we calculated the percentage of simulation time for which the minimum distance of each residue from the membrane was ≤ 5 Å for more than 5% of the simulation time (Fig. 4). In simulations of $A\beta_{1-40}$ fibrils with a membrane containing 100% DPPC, no residue binding for more than 5% of the simulation time was observed in all 20 trajectories (supplementary figure 1, 2). In $A\beta_{1-40}$ fibrils simulations with 70% DPPC-30% cholesterol membrane, out of 20 trajectories (10 each for hexamer and trimer), we detected residues of the $A\beta_{1-40}$ fibril trimer at ≤ 5 Å for more than 5% of the simulation time in 2 trajectories (SIM3 and SIM10). In both of these simulations, residues from all three chains participated in membrane binding (Fig. 5).

In both of these simulations, the binding process was mostly mediated by amino acids from the middle and the C-terminal region of the fibril (Lys16, Leu17, Val18, Phe19, Phe20, Val39, Leu34, Met35, Val36, Val39 and Val40). These residues interact with the membrane for more than 30% of the simulation time.

With a 50% DPPC-50% cholesterol membrane, we observed some residues binding to the membrane for more than 5% of the simulation time in 11 trajectories out of 20 (10 hexamers and 10 trimers). Several amino acids of the $A\beta_{1-40}$ fibrils were found to bind the membrane in 6 out of 10 hexamer simulations (SIM1, SIM4, SIM7, SIM8, SIM9 and SIM10) (Fig. 6). In particular, in SIM1, 3 chains, in SIM5 and SIM7, 5 chains, in SIM8 all 6 chains, and in SIM9 and SIM10, 4 chains participated in the binding process. In all these simulations, the strongest binding was detected for the C-terminal residues (Ile31, Leu34, Met35, Val36, Val39, Val40) and for the middle region residues (Lys16, Leu17, Val18, Phe19, Phe20). Other than these residues, binding involving N-terminal residues (Asp1, Glu3, Phe4, and Arg5) was also briefly observed (less than 30% of the simulation time) in some of the trajectories.

**Table 1**
Number of lipids in each membrane bilayers.

| Membrane bilayer | Number of DPPC molecules | Number of cholesterol molecules |
|---|---|---|
| 100% DPPC | 800 (400 in each leaflet) | 0 |
| 70% DPPC-30% cholesterol | 560 (270 in each leaflet) | 240 (120 in each leaflet) |
| 50% DPPC-30% cholesterol | 400 (200 in each leaflet) | 400 (200 in each leaflet) |

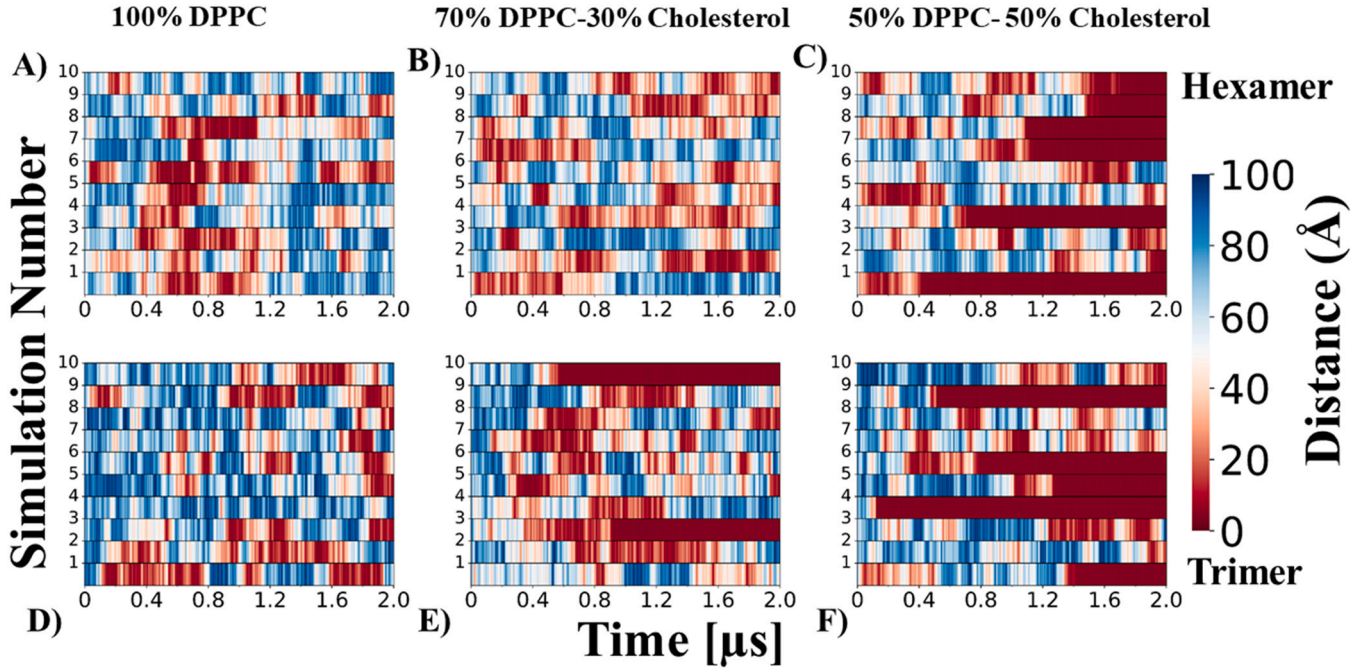


**Fig. 2.** A-C) Time evolution of the minimum distance between hexameric $A\beta_{1-40}$ fibrils and 100% DPPC, 70% DPPC-30% cholesterol and 50% DPPC-50% cholesterol membranes, respectively. D-F) Time evolution of the minimum distance between trimeric $A\beta_{1-40}$ fibrils and 100% DPPC, 70% DPPC-30% cholesterol and 50% DPPC-50% cholesterol membranes, respectively.

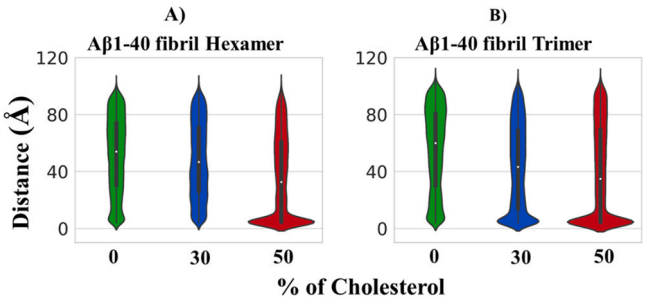


**Fig. 3.** Minimum distance violin plots for different concentrations of cholesterol in the membrane. A) $A\beta_{1-40}$ hexamer, B) $A\beta_{1-40}$ trimer.

In $A\beta_{1-40}$ fibril trimer simulations, in all five trajectories where residues were found to bind to the membrane (SIM1, SIM4, SIM5, SIM6 and SIM9) (Fig. 7), the strongest binding was observed for middle region residues (Lys16, Leu17, Val18, Phe19, Phe20) and for residues in the C-terminal region (Ile31, Ile32 Leu34, Met35, Val36, Val39, Val40). For a short period of time, binding was also observed for N-terminal residues (Asp1, Glu3, Phe4, and Arg5).

Overall, the binding to membranes containing either 30% cholesterol or 50% cholesterol involved similar $A\beta_{1-40}$ fibril residues, mostly those located in the middle region (the positively charged Lys16, the hydrophobic Leu17 and Val18, the aromatic Phe19 and Phe20) and those that are found at the C-terminus (the hydrophobic Val36, Val39, Val40, Ile31 and Met35).

### *3.3. Time evolution of the number of water, and lipid molecules around $A\beta_{1-40}$ fibrils*

To quantify the number of water molecules that a $A\beta_{1-40}$ fibril must displace to interact with the membrane, we calculated the time evolution of the number of water molecules within 6 Å of the $A\beta_{1-40}$ fibrils for all 60 independent trajectories (supplementary figure 3, 4). To interact with the membrane, $A\beta_{1-40}$ fibril hexamer lost ~150–180 water molecules and $A\beta_{1-40}$ fibril trimer lost ~120–130 water molecules. To quantify how many lipid molecules were found in the proximity of the $A\beta_{1-40}$ fibrils, we calculated the time evolution of the number of lipid molecules for all 60 trajectories. An almost negligible number of lipids remained within 6 Å of $A\beta_{1-40}$ fibrils with 100% DPPC membrane in all 20 trajectories. The same occurred when considering $A\beta_{1-40}$ fibril hexamer with a membrane containing 70% DPPC and 30% cholesterol. In the case of $A\beta_{1-40}$ fibril trimer, ~3–6 cholesterol molecules and ~6–18 DPPC molecules were found to remain within 6 Å from the membrane in the 2 trajectories (SIM3, and SIM10) in which binding occurred (Fig. 8).

In simulations involving an $A\beta_{1-40}$ fibril hexamer and a 50% DPPC-50% cholesterol membrane, we observed an almost equal number of DPPC and cholesterol lipids within 6 Å of the $A\beta_{1-40}$ fibril. Fig. 9.

In the case of $A\beta_{1-40}$ fibril trimer with a membrane containing 50% DPPC and 50% cholesterol, we noticed a generally higher number of cholesterol lipids than DPPC lipids within 6 Å of $A\beta_{1-40}$ fibrils (Fig. 10, A and B).

Overall, these data suggest that an increase in the percentage of cholesterol in the membrane leads to a greater number of cholesterol lipids within 6 Å of the membrane. This could be a possible reason for Aβ fibrils to bind more firmly to the membrane when the percentages of cholesterol and DPPC are similar.

### *3.4. Time evolution of VdW and electrostatic interaction energy between Aβ1–40 fibrils and membrane*

We studied the time evolution of VdW and electrostatic interaction energy between trimeric $A\beta_{1-40}$ fibrils and the membrane ( 70% DPPC −30% Cholestrol and 50% DPPC-50% Cholestrol) as well as between hexameric $A\beta_{1-40}$ fibrils and the membrane ( 50% DPPC −50% Cholestrol). Our results demonstrate that the binding between the membrane and the fibrils is primarily governed by VdW

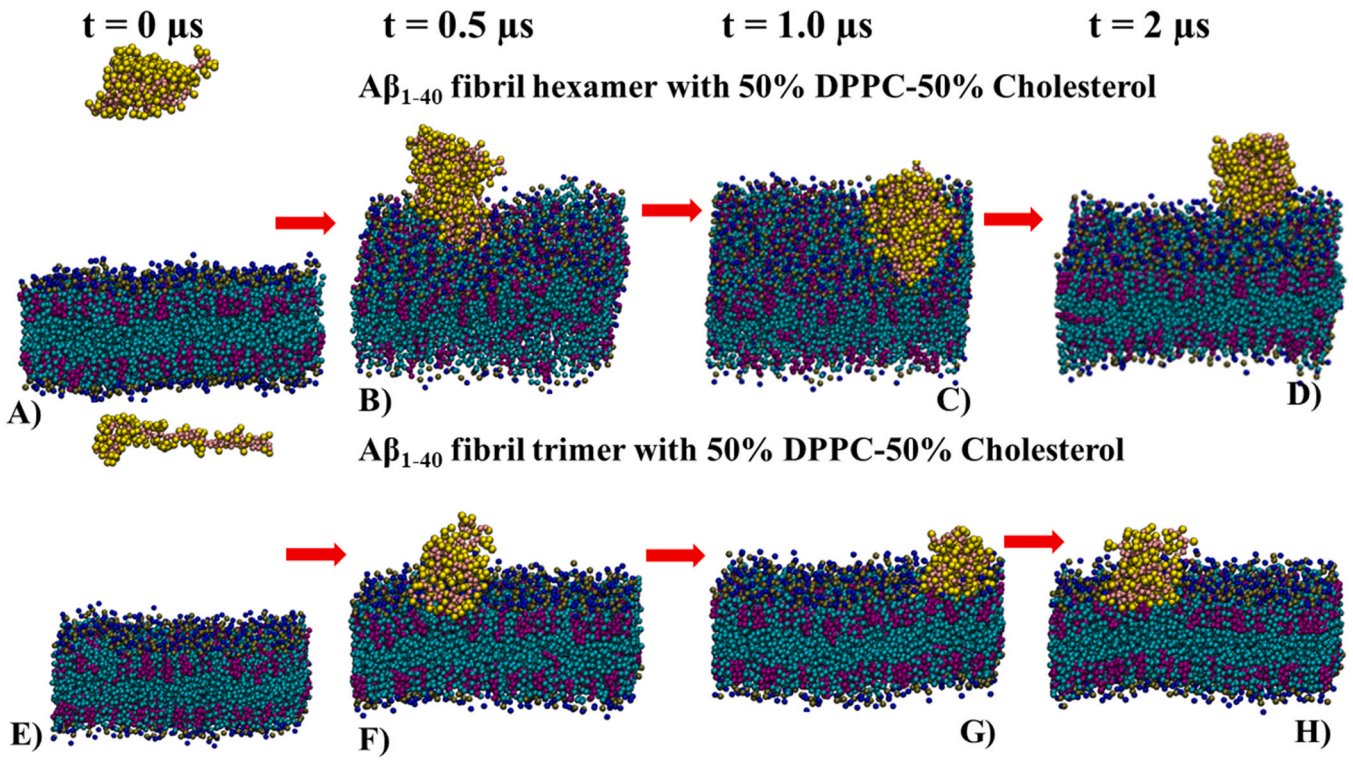


**Fig. 4.** Structures of the $A\beta_{1-40}$ fibrils with membrane containing 50% DPPC and 50% cholesterol at four different time points from two representative trajectories. A-D) Representative image for $A\beta_{1-40}$ fibril hexamer at 0, 0.5, 1.0 and 2.0 µs. E-H) Representative image for $A\beta_{1-40}$ fibril trimer at 0, 0.5, 1.0 and 2.0 µs for $A\beta_{1-40}$ fibril hexamer. $A\beta_{1-40}$ fibrils and membranes are shown in VdW representation. The backbone beads of $A\beta_{1-40}$ fibrils are depicted in pink, and the side chains beads are shown in yellow. The head group beads NC3 and PO4 of the DPPC molecules are illustrated in blue and tan, respectively, while the head group of cholesterol molecules is colored maroon. The tails of both lipid molecules are depicted in cyan.

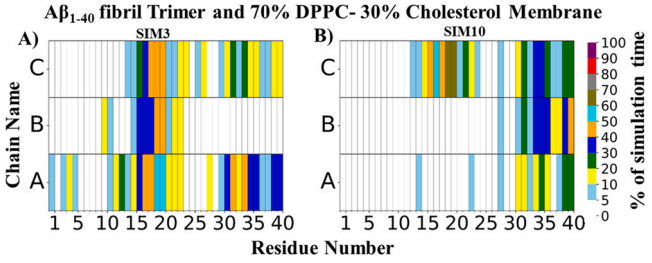


**Fig. 5.** Percentage of time in which residues of the $A\beta_{1-40}$ fibril trimer remained at a distance ≤ 5 Å from the 70% DPPC-30% cholesterol membrane in 2 out of 10 trajectories. A) SIM3, B) SIM10.

interactions and that electrostatic interactions also play a role in the binding, although to a lesser extent, as shown in Supplementary Figures 5 and 6. The VdW interaction energy was found to be in the range between ~-1000 kJ/mol to ~-2400 kJ/mol, while the electrostatic interaction energy was found to be in the range between ~-40 kJ/mol to ~-115 kJ/mol.

## 4. Discussion

In this study, we performed coarse-grained MD simulations of the interaction between an $A\beta_{1-40}$ fibril (hexamer or trimer) and a DPPC bilayer containing either no cholesterol, 30% cholesterol, or 50% cholesterol. Cholesterol is a vital component of the cell membrane and plays a critical role in maintaining its structural integrity [37]. Cholesterol makes up approximately 30–50% of the total membrane lipids in the brain, up to 50% of the overall plasma membrane [38] and up to 30% of the total lipids found in myelin [39]. Given the importance of cholesterol in the cell membrane, it is essential to investigate how Aβ fibrils bind to cell membranes containing different concentrations of cholesterol. Our simulation trajectories captured spontaneous binding of aqueous phase $A\beta_{1-40}$ fibrils with the membranes and showed that 50% cholesterol leads to a significant increase in binding events. In this study, we observed that hydrophobic residues at the C-terminus (Ile31, Ile32, Met35, Val36, Val39, and Val40) and in the middle region (Leu17, Val18, Phe19, Phe20) play a key role in the binding of the $A\beta_{1-40}$ fibrils with the membrane. This is in line with a previous study reporting that those hydrophobic residues are the most suitable for binding with lipid surfaces. Due to their hydrophobic nature, lipid surfaces accommodate the binding of such residues to reduce, to the greatest possible extent, the exposure of their acyl chains to water [40]. Lys16, which is located next to the central hydrophobic cluster (residues 17–20) has also been previously reported to interact with the cell membrane [41]. Indeed, these data are in agreement with the previous CG study of Dias et al., which showed spontaneous binding of $A\beta_{1-42}$ fibrils with membrane [21]. Our simulations reveal that both charged and hydrophobic residues participate in the binding with the membrane, in agreement also with previous studies reporting that both basic and hydrophobic amino acid residues play an important role in peripheral protein binding with the membranes [42,43]. Furthermore, we noticed that C-terminal residues significantly participate in membrane binding, which is also in line with previous studies. For instance, Khemtemourian *et. al.* [44] showed that C-terminal hydrophobic residues of islet amyloid polypeptide (IAPP) can be inserted in the membrane, while Antonschmidt *et. al.* [45] showed that α-Synuclein fibrils contain a membrane binding domain at their C-terminal edge. We also observed a loss of water molecules and an increase in the number of lipid molecules in the vicinity of the $A\beta_{1-40}$ fibrils upon membrane binding.

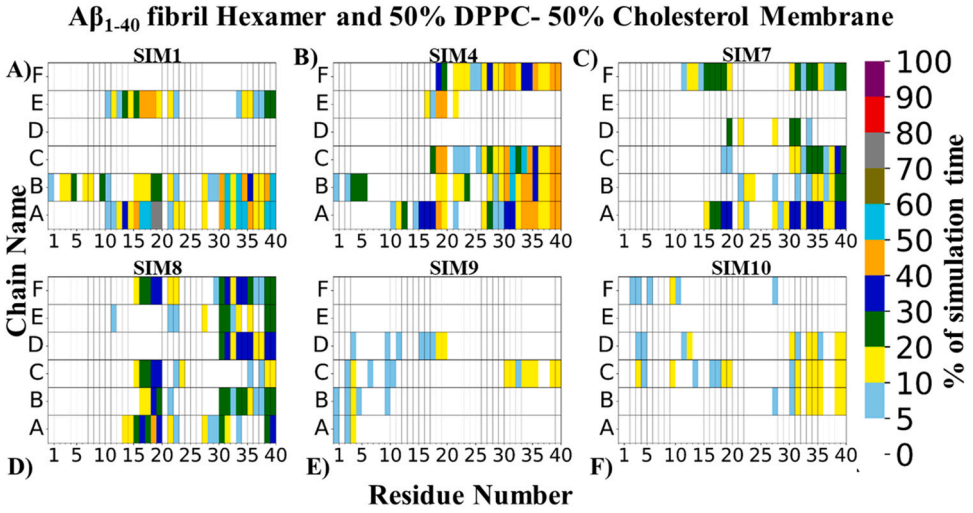


**Fig. 6.** Percentage of time in which residues of the $A\beta_{1-40}$ fibril hexamer remained at a distance ≤ 5 Å from the 50% DPPC-50% cholesterol membrane in 6 out of 10 trajectories. A) SIM1, B) SIM4. C) SIM7, D) SIM8, E) SIM9, F) SIM10.

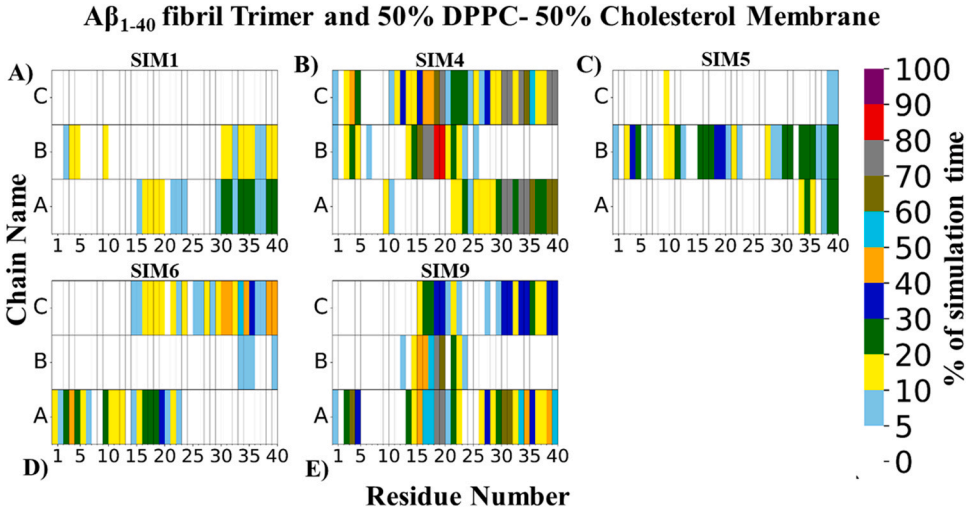


**Fig. 7.** Percentage of time in which residues of the $A\beta_{1-40}$ fibril trimer remained at a distance ≤ 5 Å from the 50% DPPC-50% cholesterol membrane in 5 out of 10 trajectories. A) SIM1, B) SIM4, C) SIM5, D) SIM6, E) SIM9.

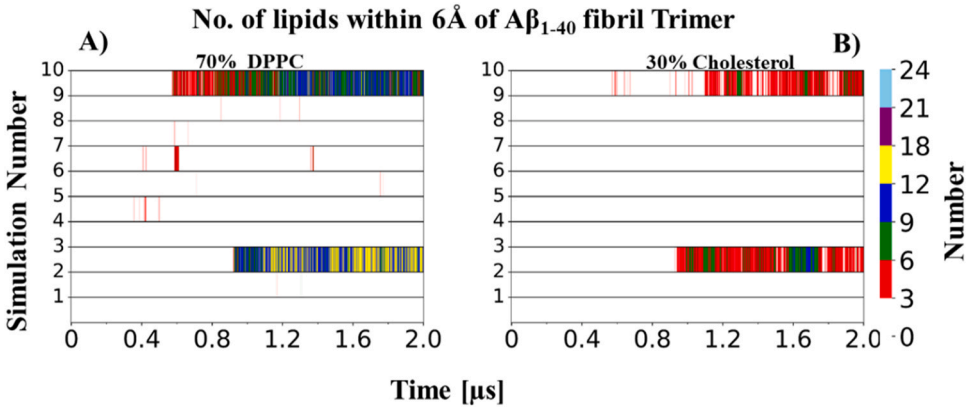


**Fig. 8.** Time evolution of the number of lipids within 6 Å of an $A\beta_{1-40}$ fibril trimer from a 70% DPPC-30% cholesterol membrane. A) DPPC, B) Cholesterol.

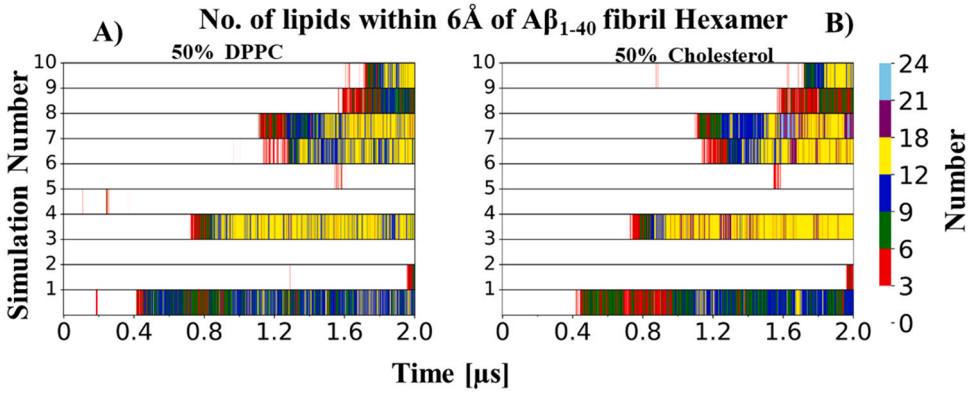


**Fig. 9.** Time evolution of the number of lipids within 6 Å of an $A\beta_{1-40}$ fibril hexamer from a 50% DPPC-50% cholesterol membrane. A) DPPC, B) Cholesterol.

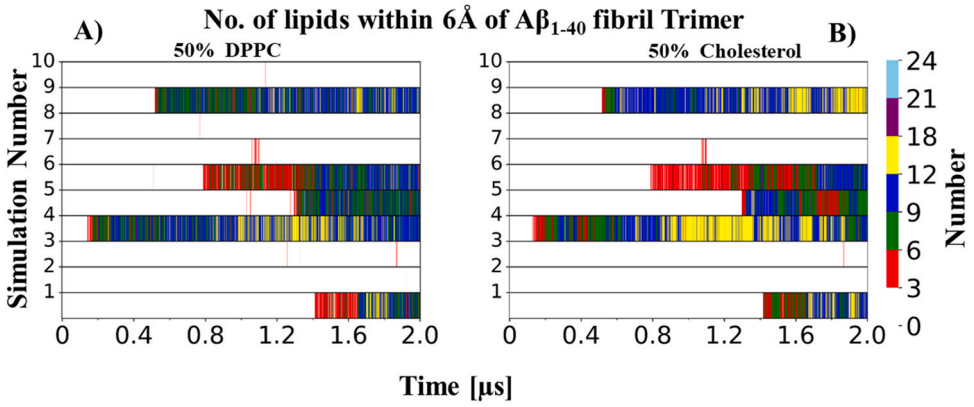


**Fig. 10.** Time evolution of the number of lipids within 6 Å of an $A\beta_{1-40}$ fibril trimer with a 50% DPPC-50% cholesterol membrane. A) DPPC, B) Cholesterol.

## 5. Conclusions

In summary, our simulations have shed light on the interaction mechanism of $A\beta_{1-40}$ fibrils with the membrane. To the best of our knowledge, this is the first report where spontaneous binding of $A\beta_{1-40}$ fibrils with a cholesterol-rich DPPC bilayer is shown. We identified key binding residues that stabilize the interaction of the $A\beta_{1-40}$ fibrils with the membrane. These findings could guide the design of new drug candidates that could inhibit the association of $A\beta_{1-40}$ fibrils with the membrane, thus opening new avenues in the design of inhibitors of the Aβ peptide-lipid membrane interaction.

## Conflict of interest

The authors declare no competing interests.

## Acknowledgments

N.A. acknowledges the ERDF postdoc grant (No. 1.1.1.2/VIAA/4/20/757) for project funding. E.P. thanks the ERDF project BioDrug (No. 1.1.1.5/19/A/004) and the Latvian Council of Science (grant No. lzp-2020/2–0013) for financial support. We would like to thank Latvian Institute of Organic Synthesis for computational resources. N.A. would also like to thank the Centre for High Performance Computing (CHPC) in Cape Town (South Africa) for supercomputing resources.

## Appendix A. Supporting information

Supplementary data associated with this article can be found in the online version at doi:10.1016/j.csbj.2023.04.013.

## References

[1] Dobson CM, Knowles TP, Vendruscolo M. The amyloid phenomenon and its significance in biology and medicine. Cold Spring Harb Perspect Biol 2020;12:a033878.
[2] Dobson CM. The amyloid phenomenon and its links with human disease. Cold Spring Harb Perspect Biol 2017;9:a023648.
[3] Chiti F, Dobson CM. Protein misfolding, amyloid formation, and human disease: a summary of progress over the last decade. Annu Rev Biochem 2017;86:27–68.
[4] Agrawal N, Parisini E. Early stages of misfolding of PAP248-286 at two different pH values: an insight from molecular dynamics simulations. Comput Struct Biotechnol J 2022;20:4892–901.
[5] Agrawal N, Skelton AA. Structure and function of Alzheimer's amyloid βeta proteins from monomer to fibrils: a mini review. Protein J 2019;38:425–34.
[6] Agrawal N, Skelton AA. 12-crown-4 ether disrupts the patient brain-derived amyloid-β-fibril trimer: insight from all-atom molecular dynamics simulations. ACS Chem Neurosci 2016;7:1433–41.
[7] Agrawal N, Skelton AA. Binding of 12-crown-4 with Alzheimer's Aβ40 and Aβ42 monomers and its effect on their conformation: insight from molecular dynamics simulations. Mol Pharm 2017;15:289–99.
[8] Quiroga IY, Cruikshank AE, Bond M, Reed K, Evangelista BA, Tseng J-H, Ragusa JV, Meeker RB, Won H, Cohen S. Synthetic amyloid beta does not induce a robust transcriptional response in innate immune cell culture systems. J Neuroinflamm 2022;19:1–12.
[9] Chiorcea-Paquim A-M, Oliveira-Brett AM. Amyloid beta peptides electrochemistry: a review, Current Opinion in. Electrochemistry 2022;31:100837.
[10] Wu T, Lin D, Cheng Y, Jiang S, Riaz MW, Fu N, Mou C, Ye M, Zheng Y. Amyloid cascade hypothesis for the treatment of alzheimer's disease: progress and challenges. AGING Dis 2022.
[11] Mullard A. Alzheimer amyloid hypothesis lives on. Nat Rev Drug Discov 2017;16:3–5.
[12] Hampel H, Hardy J, Blennow K, Chen C, Perry G, Kim SH, Villemagne VL, Aisen P, Vendruscolo M, Iwatsubo T. The amyloid-β pathway in Alzheimer's disease. Mol Psychiatry 2021;26:5481–503.
[13] Murphy MP, LeVine III H. Alzheimer's disease and the amyloid-β peptide. J Alzheimer'S Dis 2010;19:311–23.
[14] Han S, Kollmer M, Markx D, Claus S, Walther P, Fändrich M. Amyloid plaque structure and cell surface interactions of β-amyloid fibrils revealed by electron tomography. Sci Rep 2017;7:43577.

[15] Kiskis J, Fink H, Nyberg L, Thyr J, Li J-Y, Enejder A. Plaque-associated lipids in Alzheimer's diseased brain tissue visualized by nonlinear microscopy. Sci Rep 2015;5:13489.
[16] Burns MP, Noble WJ, Olm V, Gaynor K, Casey E, LaFrancois J, Wang L, Duff K. Co-localization of cholesterol, apolipoprotein E and fibrillar Aβ in amyloid plaques. Mol Brain Res 2003;110:119–25.
[17] Yu X, Wang Q, Pan Q, Zhou F, Zheng J. Molecular interactions of Alzheimer amyloid-β oligomers with neutral and negatively charged lipid bilayers. Phys Chem Chem Phys 2013;15:8878–89.
[18] Tofoleanu F, Buchete N-V. Molecular interactions of Alzheimer's Aβ protofilaments with lipid membranes. J Mol Biol 2012;421:572–86.
[19] Tofoleanu F, Brooks BR, Buchete N-V. Modulation of Alzheimer's Aβ protofilament-membrane interactions by lipid headgroups. ACS Chem Neurosci 2015;6:446–55.
[20] Dong X, Sun Y, Wei G, Nussinov R, Ma B. Binding of protofibrillar Aβ trimers to lipid bilayer surface enhances Aβ structural stability and causes membrane thinning. Phys Chem Chem Phys 2017;19:27556–69.
[21] Dias CL, Jalali S, Yang Y, Cruz L. Role of cholesterol on binding of amyloid fibrils to lipid bilayers. J Phys Chem B 2020;124:3036–42.
[22] Fändrich M, Nyström S, Nilsson KPR, Böckmann A, LeVine III H, Hammarström P. Amyloid fibril polymorphism: a challenge for molecular imaging and therapy. J Intern Med 2018;283:218–37.
[23] Meinhardt J, Sachse C, Hortschansky P, Grigorieff N, Fändrich M. Aβ (1-40) fibril polymorphism implies diverse interaction patterns in amyloid fibrils. J Mol Biol 2009;386:869–77.
[24] Paravastu AK, Leapman RD, Yau W-M, Tycko R. Molecular structural basis for polymorphism in Alzheimer's β-amyloid fibrils. Proc Natl Acad Sci 2008;105:18349–54.
[25] Ghosh U, Thurber KR, Yau W-M, Tycko R. Molecular structure of a prevalent amyloid-β fibril polymorph from Alzheimer's disease brain tissue. Proc Natl Acad Sci 2021;118:e2023089118.
[26] Jo S, Kim T, Iyer VG, Im W. CHARMM-GUI: a web-based graphical user interface for CHARMM. J Comput Chem 2008;29:1859–65.
[27] Qi Y, Ingólfsson HI, Cheng X, Lee J, Marrink SJ, Im W. CHARMM-GUI martini maker for coarse-grained simulations with the martini force field. J Chem Theory Comput 2015;11:4486–94.
[28] de Jong DH, Singh G, Bennett WD, Arnarez C, Wassenaar TA, Schafer LV, Periole X, Tieleman DP, Marrink SJ. Improved parameters for the martini coarse-grained protein force field. J Chem Theory Comput 2013;9:687–97.
[29] Marrink SJ, Risselada HJ, Yefimov S, Tieleman DP, De AH. Vries, The MARTINI force field: coarse grained model for biomolecular simulations. J Phys Chem B 2007;111:7812–24.
[30] Bixon M, Lifson S. Potential functions and conformations in cycloalkanes. Tetrahedron 1967;23:769–84.
[31] Parrinello M, Rahman A. Polymorphic transitions in single crystals: a new molecular dynamics method. J Appl Phys 1981;52:7182–90.
[32] Bussi G, Donadio D, Parrinello M. Canonical sampling through velocity rescaling. J Chem Phys 2007;126:014101.
[33] Abraham MJ, Murtola T, Schulz R, Páll S, Smith JC, Hess B, Lindahl E. GROMACS: high performance molecular simulations through multi-level parallelism from laptops to supercomputers. SoftwareX 2015;1:19–25.
[34] Buchoux S. FATSLiM: a fast and robust software to analyze MD simulations of membranes. Bioinformatics 2017;33:133–4.
[35] Bharadwaj P, Solomon T, Malajczuk CJ, Mancera RL, Howard M, Arrigan DW, Newsholme P, Martins RN. Role of the cell membrane interface in modulating production and uptake of Alzheimer's beta amyloid protein. Biochim Et Biophys Acta (BBA)-Biomembr 2018;1860:1639–51.
[36] Butterfield SM, Lashuel HA. Amyloidogenic protein–membrane interactions: mechanistic insight from model systems. Angew Chem Int Ed 2010;49:5628–54.
[37] Zhang J, Li Q, Wu Y, Wang D, Xu L, Zhang Y, Wang S, Wang T, Liu F, Zaky MY. Cholesterol content in cell membrane maintains surface levels of ErbB2 and confers a therapeutic vulnerability in ErbB2-positive breast cancer. Cell Commun Signal 2019;17:1–12.
[38] Risselada HJ. Cholesterol: the plasma membrane's constituent that chooses sides. Biophys J 2019;116:2235.
[39] Ho WY, Hartmann H, Ling SC. Central nervous system cholesterol metabolism in health and disease. IUBMB life 2022;74:826–41.
[40] Srivastava AK, Pittman JM, Zerweck J, Venkata BS, Moore PC, Sachleben JR, Meredith SC. β-Amyloid aggregation and heterogeneous nucleation. Protein Sci 2019;28:1567–81.
[41] Sinha S, Lopes DH, Bitan G. A key role for lysine residues in amyloid β-protein folding, assembly, and toxicity, ACS Chemical. Neuroscience 2012;3:473–81.
[42] Fuglebakk E, Reuter N. A model for hydrophobic protrusions on peripheral membrane proteins. PLoS Comput Biol 2018;14:e1006325.
[43] Larsen AH, John LH, Sansom MS, Corey RA. Specific interactions of peripheral membrane proteins with lipids: what can molecular simulations show us? Biosci Rep 2022;42.
[44] Khemtemourian L, Fatafta H, Davion B, Lecomte S, Castano S, Strodel B. Structural dissection of the first events following membrane binding of the islet amyloid polypeptide. Front Mol Biosci 2022;9:849979.
[45] Antonschmidt L, Dervişoğlu R, Sant V, Tekwani Movellan K, Mey I, Riedel D, Steinem C, Becker S, Andreas LB, Griesinger C. Insights into the molecular mechanism of amyloid filament formation: Segmental folding of α-synuclein on lipid membranes. Sci Adv 2021;7:eabg2174.